Statistical Finite Elements for Vibration Problems

Timothy J. Rogers — *Dynamics Research Group, University of Sheffield, UK*
Brandon J. O'Connell — *Dynamics Research Group, University of Sheffield, UK*
Max D. Champneys — *Dynamics Research Group, University of Sheffield, UK*

Abstract

Finite element (FE) methods remain one of the most widely used approaches across science and engineering for computing numerical solutions to partial differential equations. Given their widespread use, it is a natural family of methods to be considered within the framework of probabilistic numerics. Previous work has introduced the "statistical finite element method" (statFEM) as a tool for coherent treatment of uncertainty when working with FE models. Current formulations of statFEM rely on the discretised system being represented by a linear system of equations which is then solved. Within the scope of FE approaches there exists an alternative solution for cases where the modeller wishes to investigate the dynamic properties, i.e. resonant frequencies and associated mode shapes, of a system. Recovery of these properties requires solving a generalised eigenvalue problem utilising the discretised mass and stiffness matrices. The contribution of this work is to show how the approach of statFEM may be readily expanded to also cover this case by forming an approximate distribution over the eigenvalues and eigenvectors given a random field prior over one or more of the model properties chosen as a Gaussian process. We demonstrate the effectiveness of this approach on the classic test case of a cantilevered beam showing the approximated uncertainty recovered over both the eigenvalues and the eigenvectors.

Proceedings of the 2nd International Conference on Probabilistic Numerics (ProbNum) 2026, Lappeenranta, Finland. PMLR Volume 341.

1 Introduction

The finite element method (FEM) for numerical solutions to partial differential equations (PDEs) remains one of the most widely adopted techniques across science and engineering. Therefore, for those interested in uncertainty quantification, it is an important topic for consideration. Within the scope of probabilistic numerics (Hennig et al., 2015), interest in FEM is no exception with the key contribution being that of the statistical Finite Element Method (statFEM) of Girolami et al. (2021).

Under the model of statFEM, multiple sources of uncertainty are unified to provide a coherent approach. The four key sources of uncertainty which are included are parameter uncertainty (as a random field), load uncertainty, model discrepancy and measurement noise. These are combined to provide a complete description of the uncertainty for both forward and inverse modelling problems. A brief mathematical introduction to statFEM is presented in Section 2.

Current studies using statFEM have predominantly focused on "static" problems, i.e. the solution to spatial PDEs subject to a (temporally) constant load and neglecting their inertia. In the context of structural mechanics, the strong form of the static PDE will be,

$$-\nabla \cdot \sigma = f \tag{1}$$

with σ being the stress tensor and f being the loading. In these static problems, applying FEM reduces the PDE to solving a linear system of equations of the form $A(\boldsymbol{\theta})\boldsymbol{u} = \boldsymbol{f}$, with parameters $\boldsymbol{\theta}$ and load $\boldsymbol{f}$, such that a distribution over $\boldsymbol{u}$ can be recovered (at least approximately). Such solutions correspond, for example, to steady-state thermal problems or static solid mechanics. Note that here we restrict ourselves to the setting of linear FEM methods; in the nonlinear case, some further operations are needed, but this topic lies beyond the scope of this paper. The interested reader is directed towards (e.g.) Bathe (2006).

In contrast, engineers are often interested in the *dynamic* response of a system for which the strong form PDE also contains a term corresponding to the inertia:

$$\rho \frac{\partial^2 u}{\partial t^2} - \nabla \cdot \sigma = f, \tag{2}$$

with the added complication that the system is now evolving spatio-temporally. For ease of exposition we neglect damping. The FEM procedure yields the discretised equations,

$$M\ddot{\boldsymbol{u}} + K\boldsymbol{u} = \boldsymbol{f}, \tag{3}$$

with mass matrix M and stiffness matrix K, overdots are used for time derivatives.

In seeking a numerical solution to these dynamic problems, the simplest approach is to perform a time-stepping solution. The challenge in such a setting is that numerical integration must be performed for the spatio-temporal solution. For example, one could use Runge-Kutta or Newmark integration, which is often favoured for these second-order systems. Equation (3) is typically a very large system of coupled second-order ordinary differential equations (ODEs). For even modest engineering models, the length of vector $\boldsymbol{u}$ (the degrees-of-freedom, or DOFs) may be of the order of 10^5. In the statFEM literature, this explicit integration has been the only approach currently explored. For example, see Duffin et al. (2022) where low-rank approximations of

the covariance are required to manage the computational load.

However, within traditional FEM/dynamics techniques an alternative is to target directly the dominant eigenvalues and eigenvectors of the discretised PDE. Each value-vector pair forming one *eigenmode* or *eigenpair* (in mechanics this is commonly shortened to simply "mode"). The eigendecomposition is equivalent to solving the homogeneous solution of the system of ODEs, independent of a specific forcing profile. Following computation of the eigenmodes, simulation can be achieved efficiently for a given forcing by means of "modal superposition" (Rao and Yap (1995)). We provide a brief introduction to the concepts of "modal analysis" in Appendix A.

The eigenmodes also have a tangible interpretation in the context of vibration problems where the eigenvalue corresponds to the square of the resonant frequency. The eigenvector corresponds to the "mode shape" or characteristic pattern of movement of the system, when excited harmonically at the associated resonant frequency. Recovering this (eigen-)modal solution is computationally favourable and generally more interpretable than the explicit dynamics approach. It provides a separation between the intrinsic dynamic properties of the system (its resonance frequencies and eigenfunctions) and the time response to a specific forcing profile. In a design setting, for example, an engineer is generally more concerned with ensuring that resonance in the system does not coincide with some known excitation (e.g. rotating machinery) than simulating the response to individual realisations of loading signals. Therefore, developing a form of statFEM which may be applicable for such vibration problems based on the eigendecomposition of the discretised PDE is our current contribution.

Notation: we will use bold face ($\boldsymbol{a}$) to indicate vectors, capitalisation (A) for matrix valued quantities, $(\cdot)^{\mathrm{T}}$ for matrix transposes, and $(\cdot)^{\dagger}$ for the Moore-Penrose pseudo-inverse. $\mathbb{I}$ is the identity matrix.

1.1 Related Works

Work in statFEM stems from the contribution of Girolami et al. (2021) where both the forward and inverse problems are addressed using a one-dimensional steady-state Poisson problem as an exemplar FEM application. Following this first introduction, discussion of the theoretical guarantees afforded by adopting the statFEM approach has received attention, e.g. Papandreou et al. (2023); Duffin et al. (2026) — these works have also concentrated on the behaviour of statFEM in the static case.

There has been work considering alternative approximations within the forward problem of statFEM, which is generally intractable. Akyildiz et al. (2022) employ Langevin dynamics to sample from the distribution over the solution $\boldsymbol{u}$ when parameters in the PDE are defined as random fields, using a Gaussian process prior. Barros et al. (2025) presented an alternative approach for approximating the distribution over the solution in the forward modelling case through the use of a Copula process approach, again shown on a steady-state Poisson problem.

The approach was later shown to be effective in structural mechanics settings. Sun et al. (2023) show that statFEM provides an effective means for forward and inverse problems in rail buckling where observations from fibre-optic sensing systems are available. Within a civil engineering context, Febrianto et al. (2022) demonstrate the application of statFEM to a bridge structure in the UK where fibre sensing is again employed to provide observations with which the model may be updated.

Although there are currently no applications of statFEM for (eigen-)modal dynamic analysis, management of uncertainty through eigenvalue problems has been considered within the structural dynamics community. For example, Adhikari and Friswell (2007) discuss methods for discrete dynamic systems — including Taylor series approximations of the statistical moments. Furthermore, there has been extensive use of random matrix theory (e.g. Soize (2005); Cicirello and Langley (2013)). However, none of these works directly address the problem of random fields defined on a finite element model.

2 statFEM

Girolami et al. (2021) introduced the Statistical Finite Element Method (statFEM), a hierarchical Bayesian framework for finite element modelling that coherently incorporates uncertainty from spatially varying PDE parameters, applied forcing fields, and model discrepancy.

There are four sources of uncertainty considered in the formulation of statFEM which give rise to a combined picture of uncertainty in the forward problem and enable a consistent approach to the inverse problem. These sources are: the model is subject to parameters modelled as a random field (chosen to be a Gaussian process) across the domain; the load vector is also modelled as a Gaussian process; there is an additive model discrepancy between the output of the finite element model and the observed data; and there is measurement noise corrupting the observed quantities. Mathematically, the model can be written:

$$\boldsymbol{y}(\boldsymbol{x},\boldsymbol{\theta}) = \rho P\boldsymbol{u}(\boldsymbol{x},\boldsymbol{\theta}) + \boldsymbol{d}(\boldsymbol{x}) + \boldsymbol{e}, \tag{4}$$

where the observed data $\boldsymbol{y}(\boldsymbol{x},\boldsymbol{\theta})$ is described at a location in the domain $\boldsymbol{x}$, given some spatially (randomly) varying parameter $\boldsymbol{\theta}(\boldsymbol{x})$ (we drop the explicit dependency of $\boldsymbol{\theta}$ on $\boldsymbol{x}$ for compactness). The observations are assumed to arise as a result of some physical process which is simulated (i.e. the FE model). The nodal solutions $\boldsymbol{u}(\boldsymbol{x},\boldsymbol{\theta})$ are scaled by ρ and projected by a matrix P onto the observation. In the simplest case, P is a binary matrix which selects the nodes where observations are made, although it can also be used to (linearly) interpolate the mesh or, for example, recover a distribution over element strains. Since not all physical

mechanisms will be captured in $\boldsymbol{u}$, statFEM also allows for a spatially dependent *discrepancy* model $\boldsymbol{d}(\boldsymbol{x})$. Finally, the observations are assumed to be corrupted by noise $\boldsymbol{e}$.

In statFEM, the discrepancy is assumed to be a Gaussian process (as in Kennedy and O'Hagan (2001)), and the noise to be independent additive Gaussian white noise with a fixed variance. Since both of these are Gaussian distributed random variables, their summation is straightforward. The recovery of a distribution over $\boldsymbol{u}$ is more challenging. In the FEM procedure, the PDE being modelled is reduced to a linear system

$$A(\boldsymbol{\theta})\boldsymbol{u} = \boldsymbol{f}, \tag{5}$$

with $A(\boldsymbol{\theta})$ being a "stiffness matrix" dependent on the parameter $\boldsymbol{\theta}$ and $\boldsymbol{f}$ being the applied loads to the system (in structural mechanics terms). Separate Gaussian process priors are placed over $\boldsymbol{\theta}$ and $\boldsymbol{f}$ in the general case such that:

$$\boldsymbol{\theta}(\boldsymbol{x}) \sim \mathcal{GP}\left(\bar{\boldsymbol{\theta}}(\boldsymbol{x}), c_{\boldsymbol{\theta}}(\boldsymbol{x}, \boldsymbol{x}')\right), \tag{6}$$

$$\boldsymbol{f}(\boldsymbol{x}) \sim \mathcal{GP}\left(\bar{\boldsymbol{f}}(\boldsymbol{x}), c_{\boldsymbol{f}}(\boldsymbol{x}, \boldsymbol{x}')\right). \tag{7}$$

Computing the distribution over $\boldsymbol{u}$ is not possible in closed form since the inversion of $A(\boldsymbol{\theta})$ is a highly nonlinear operation. Therefore, a Taylor series method to compute the first two moments of $\boldsymbol{u}$ is used to arrive at an approximate Gaussian distribution over $\boldsymbol{u}$:

$$p(\boldsymbol{u} \mid \boldsymbol{\theta}, \boldsymbol{f}) \approx \mathcal{N}(\bar{\boldsymbol{u}}, C_u), \tag{8}$$

where $\bar{\boldsymbol{u}} = A(\bar{\boldsymbol{\theta}})^{-1}\bar{\boldsymbol{f}}$ and

$$\begin{aligned} C_u =& A(\bar{\boldsymbol{\theta}})^{-1} C_{\boldsymbol{f}} A(\bar{\boldsymbol{\theta}})^{-\mathrm{T}} + \\ & \sum_{e=1}^{n_e}\sum_{d=1}^{n_e} (C_{\boldsymbol{\theta}})_{ed} B_e \left(C_{\boldsymbol{f}} + \bar{\boldsymbol{f}} \otimes \bar{\boldsymbol{f}}\right) B_d^{\mathrm{T}}, \end{aligned} \tag{9}$$

with the sensitivity matrices defined for each element $e \in \{1, \ldots, n_e\}$ as

$$B_e = A(\bar{\boldsymbol{\theta}})^{-1} \frac{\partial A(\bar{\boldsymbol{\theta}})}{\partial \theta_e} A(\bar{\boldsymbol{\theta}})^{-1}. \tag{10}$$

Now, with a Gaussian approximation over $\boldsymbol{u}$, the distribution over $\boldsymbol{y}$ is straightforward to write down knowing sums and affine transformations of Gaussians. This gives a statFEM model which is appropriate for many FEM tasks including, in a mechanics setting, the recovery of displacements in a system subject to *static* loads. Following a similar line of reasoning, our contribution in the next section is to the *dynamic* case where one is interested in the eigenmodes of the FE model.

3 Eigendecomposition in statFEM

Considering now the structural vibration setting, the goal will be to find (a subset of) the eigenmodes of the structural system. We will follow similarly to statFEM, specifically the case where there exists a random field over one or more of the physical properties of the system ($\boldsymbol{\theta}$) and the goal is to compute an (approximate) posterior over its eigenvalues ($\boldsymbol{\lambda}$) and the eigenvector matrix $\Phi = [\boldsymbol{\phi}_1, \ldots, \boldsymbol{\phi}_Q]$, comprising pairs $\{\lambda_i, \boldsymbol{\phi}_i\}_{i=1}^{Q}$. By convention we will order these eigenpairs by ascending eigenvalue and choose a number of pairs Q which is typically much less than the total number of degrees of freedom in the model. Note that targeting the eigenvalue problem changes the nonlinear transformation through which the parameter distribution must be propagated.

Following the usual finite element discretisation procedure, the PDE is reduced to a generalised eigenvalue problem:

$$K(\boldsymbol{\theta})\boldsymbol{\phi}_i = \lambda_i M(\boldsymbol{\theta})\boldsymbol{\phi}_i, \quad i = 1, \ldots, Q, \tag{11}$$

where both the mass ($M(\boldsymbol{\theta})$) and stiffness ($K(\boldsymbol{\theta})$) matrices are functions of the physical properties of the system, e.g. elastic modulus, density, thickness. Again, a GP prior over $\boldsymbol{\theta}$ is also chosen such that,

$$\boldsymbol{\theta}(\boldsymbol{x}) \sim \mathcal{GP}\left(\bar{\boldsymbol{\theta}}(\boldsymbol{x}), c_{\boldsymbol{\theta}}(\boldsymbol{x}, \boldsymbol{x}')\right) \tag{12}$$

for some mean function $\bar{\boldsymbol{\theta}}(\boldsymbol{x})$ and covariance function $c_{\boldsymbol{\theta}}(\boldsymbol{x}, \boldsymbol{x}')$ evaluated at points $\boldsymbol{x}$ and $\boldsymbol{x}'$ in the input domain.

The quantity of interest will then be

$$p(\boldsymbol{\lambda}, \Phi) = \int p(\boldsymbol{\lambda}, \Phi \mid \boldsymbol{\theta}) p(\boldsymbol{\theta}) \mathrm{d}\boldsymbol{\theta}, \tag{13}$$

with $p(\boldsymbol{\theta}) = \mathcal{N}\left(\bar{\boldsymbol{\theta}}\left(\boldsymbol{X}^{(c)}\right), C_{\boldsymbol{\theta}}\left(\boldsymbol{X}^{(c)}, \boldsymbol{X}^{(c)}\right)\right)$ which corresponds to the prior over $\boldsymbol{\theta}$ being evaluated at all pairs of element barycentres $\boldsymbol{X}^{(c)}$.

Since the solution to the eigenvalue problem in Eq. (11) is a nonlinear operation, the integral in Eq. (13) will be intractable. As in Girolami et al. (2021), a perturbation approach is adopted to avoid the computational load of, e.g., Monte Carlo approximation of Eq. (13) given that $\boldsymbol{\theta}$ will likely be high dimensional.

The core approach of the approximation used will be to consider a series expansion of the quantity of interest which is considered up to the first order; see Girolami et al. (2021); Liu et al. (1986). The key results for the approximate first two moments of the eigenvalues and eigenvectors will now be shown. See Appendix B for details on the series expansion and Appendix C for more details on the required derivatives of the eigenvalue problem w.r.t. the uncertain parameter.

For compactness of notation, we define the mass and stiffness matrices evaluated at the mean parameter field as $\bar{M} \triangleq M(\bar{\boldsymbol{\theta}})$ and $\bar{K} \triangleq K(\bar{\boldsymbol{\theta}})$. Note that because the mapping from parameters to the system matrices is generally non-linear, $\bar{M}$ and $\bar{K}$ are first-order approximations to the true expected matrices $\mathbb{E}[M]$ and $\mathbb{E}[K]$. Following the first-order Taylor series expansion, the zeroth-order approximations for the expected eigenvalues and eigenvectors are obtained by solving the deterministic generalised eigenvalue problem evaluated at the mean parameter field:

$$\bar{K}\bar{\boldsymbol{\phi}}_i = \bar{\lambda}_i \bar{M}\bar{\boldsymbol{\phi}}_i, \quad i = 1, \ldots, Q, \tag{14}$$

the mean eigenvalue matrix is $\bar{\Lambda} = \mathrm{diag}(\bar{\lambda}_1, \ldots, \bar{\lambda}_Q)$ and the corresponding mean eigenvector matrix is $\bar{\Phi} = [\bar{\boldsymbol{\phi}}_1, \ldots, \bar{\boldsymbol{\phi}}_Q]$.

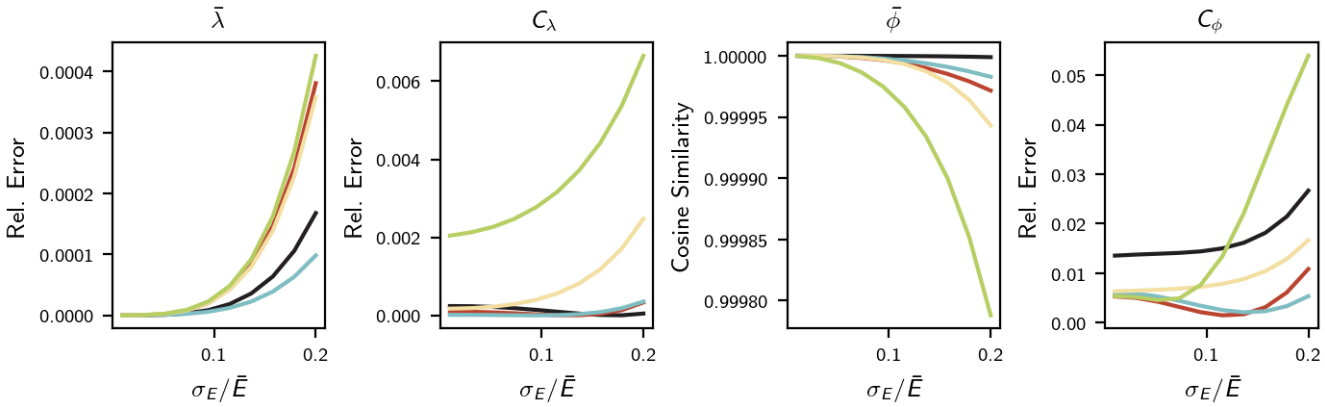

Figure 1: Comparison of Taylor series approximation with Monte Carlo estimates for the first five eigenmodes. From left to right: first moment of the eigenvalues ($\bar{\lambda}$), second moment of the eigenvalues (C_λ), first moment of the eigenvectors ($\bar{\phi}$) and second moment of the eigenvectors (C_ϕ) with colours corresponding to the eigenpair with values λ_1 (—), λ_2(—), λ_3 (—), λ_4 (—), λ_5 (—).

3.1 Eigenvalues

What follows is to compute the covariance of the eigenvalues such that an approximation to their distribution can be achieved. Leveraging the series approximation of the eigenvalues and after quite some manipulation, the following expression for the covariance between the i^{th} and j^{th} eigenvalue can be recovered:

$$\begin{aligned}\mathrm{Cov}(\lambda_i, \lambda_j) = \sum_{e=1}^{n_e}\sum_{d=1}^{n_e} C_{ed}^{\boldsymbol{\theta}} \left[\bar{\boldsymbol{\phi}}_i^{\mathrm{T}} \left(\frac{\partial \bar{K}}{\partial \theta_e} - \bar{\lambda}_i \frac{\partial \bar{M}}{\partial \theta_e}\right) \bar{\boldsymbol{\phi}}_i\right] \\ \times \left[\bar{\boldsymbol{\phi}}_j^{\mathrm{T}} \left(\frac{\partial \bar{K}}{\partial \theta_d} - \bar{\lambda}_j \frac{\partial \bar{M}}{\partial \theta_d}\right) \bar{\boldsymbol{\phi}}_j\right]\end{aligned} \tag{15}$$

As a note on implementation, it is typical that $\bar{K}$ will be very sparse which can and should be exploited. Furthermore, consider the derivative $\frac{\partial \bar{K}}{\partial \theta_e}$. This quantity will only be non-zero in degrees of freedom (DOFs) related to nodes in element e. As such, the computation of the inner product,

$$\bar{\boldsymbol{\phi}}_i^{\mathrm{T}} \left(\frac{\partial \bar{K}}{\partial \theta_e} - \bar{\lambda}_i \frac{\partial \bar{M}}{\partial \theta_e}\right) \bar{\boldsymbol{\phi}}_i, \tag{16}$$

should be replaced by indexing the relevant DOFs in $\bar{\boldsymbol{\phi}}_i$ and using only the element stiffness or element mass matrix derivatives rather than the full matrices.

3.2 Eigenvectors

The expression for the covariance of eigenvector $\boldsymbol{\phi}_i$ and eigenvector $\boldsymbol{\phi}_j$ is significantly more involved although conceptually follows the same procedure. We begin by defining

$$F_i = -\bar{\Phi}\left(\bar{\Lambda} - \bar{\lambda}_i \mathbb{I}\right)^{\dagger} \bar{\Phi}^{\mathrm{T}}, \tag{17}$$

where $(\cdot)^{\dagger}$ denotes the Moore-Penrose pseudo-inverse, which is required since the matrix $\left(\bar{\Lambda} - \bar{\lambda}_i \mathbb{I}\right)$ is singular (and hence not invertible). We also define,

$$D_{ei} = \left(\frac{\partial \bar{K}}{\partial \theta_e} - \bar{\lambda}_i \frac{\partial \bar{M}}{\partial \theta_e}\right) - \frac{1}{2}\left(\bar{\boldsymbol{\phi}}_i^{\mathrm{T}} \frac{\partial \bar{M}}{\partial \theta_e} \bar{\boldsymbol{\phi}}_i\right) \bar{M}, \tag{18}$$

$$\tilde{C}_{ij}^{(ed)} = \bar{\boldsymbol{\phi}}_i C_{ed}^{\boldsymbol{\theta}} \bar{\boldsymbol{\phi}}_j^{\mathrm{T}}. \tag{19}$$

D_{dj} is equivalent to D_{ei} but replacing subscripts e with d and i with j. Also note that F_j, D_{dj} are symmetric but transposes are shown for clarity in the following expression.

Now an expression for the covariance between $\boldsymbol{\phi}_i$ and $\boldsymbol{\phi}_j$ can be shown to be,

$$\mathrm{Cov}(\boldsymbol{\phi}_i, \boldsymbol{\phi}_j) = \sum_{e=1}^{n_e}\sum_{d=1}^{n_e} F_i D_{ei} \tilde{C}_{ij}^{(ed)} D_{dj}^{\mathrm{T}} F_j^{\mathrm{T}} \tag{20}$$

As when considering the eigenvalues, the computational burden of Eq. (20) is greatly reduced by exploiting the very high degree of sparsity in the partial derivatives of M and K w.r.t. the parameters.

With these two expressions in place, it is possible to approximate the distribution over the eigenvalues and eigenvectors as a Gaussian distribution. If desired, a discrepancy function can also be added in the case where observations of the eigenvectors have been made via some identification procedure.

3.3 Implementation Details

As mentioned, to provide efficient computation of the statFEM solution, it is very favourable to exploit sparsity in the quantities which are needed for the covariance calculations. Noting that for these covariances there is a double sum over the number of elements, reducing operations inside this step is important.

Trivially, in the case where the parameter only affects either the stiffness K or the mass M, terms related to the derivative of the other can be removed. For example, if only the elastic modulus E is modelled as a GP then all terms $\frac{\partial \bar{M}}{\partial \theta_e}$ are 0 (and similarly for the d^{th} element). This greatly simplifies, for example, $D_{ei} = \frac{\partial \bar{K}}{\partial \theta_e} \bar{\boldsymbol{\phi}}_i$.

The other critical optimisation arises from the realisation that the derivative terms,

$$\frac{\partial \bar{M}}{\partial \theta_e}, \; \frac{\partial \bar{K}}{\partial \theta_e}, \tag{21}$$

will be highly sparse. Only the degrees of freedom associated with the element e or d will be non-zero in the

derivative. Therefore, we should compute the *element* stiffness or mass derivatives

$$\frac{\partial \bar{M}_e}{\partial \theta_e}, \frac{\partial \bar{K}_e}{\partial \theta_e}, \tag{22}$$

which will have much lower dimension. Then, if `dofs_e` are the degrees of freedom associated with element e, the computation of Eq. (16) for element e for all i can be written,

```
inner = dke[..., None]- \
        lam[None,None]*dme[...,None]
dlde = jnp.einsum(
         "ni, nmi, mi -> i",
         phi[dofs_e], inner, phi[dofs_e]
       )
```

where we broadcast across the number of eigenmodes then this operation is vectorised across the number of elements using `vmap` in JAX (Bradbury et al. (2018)).

4 Results

We begin with a small FE model on which we perform a Monte Carlo analysis to determine the effectiveness of the proposed Taylor series approximation for the distribution over the eigendecomposition. We choose a simple rectangular domain of size 1m by 0.5m, and choose the lower left corner as the origin for the global coordinate system ($x = 0$m, $y = 0$m). This domain is divided into 15 elements along x and 2 elements along its shorter side, y. This configuration leads to a mesh size of 30 elements and 125 nodes; each node has two degrees of freedom. Each of the elements is chosen as 8-node quadrilaterals with second-order shape functions (the "serendipity-quad"); details of the element formulation are given in Appendix D.

A "cantilever"-type boundary is applied, which is equivalent to a Dirichlet condition with zero displacement constraints in both directions at all nodes falling on the left-hand edge of the domain, i.e. at $x = 0$. For this initial study we select the density $\rho = 1.0\text{kg}\,\text{m}^{-3}$ and model the elastic modulus E to vary according to the following GP, i.e. $\theta = E$,

$$E \sim \mathcal{GP}(\bar{E}, c_E(\boldsymbol{x}, \boldsymbol{x}')) \tag{23}$$

where we collect $\boldsymbol{x} = (x, y)$ and $\bar{E} = 100$Pa. The covariance function is chosen to be the commonly adopted squared exponential covariance function,

$$c_E(\boldsymbol{x}, \boldsymbol{x}') = \sigma_E^2 \cdot e^{-\frac{||\boldsymbol{x}-\boldsymbol{x}'||^2}{2\ell^2}}. \tag{24}$$

We will fix the lengthscale of this covariance function to $\ell = 0.01$ and vary the value of σ_E^2 to investigate the effect of increasing uncertainty on the quality of the approximation given by the Taylor series. We note that, unlike Girolami et al. (2021), we do not apply an additional nonlinear transformation on E before its inclusion in the FEM calculations, although this is trivial to include if the user desired.

In the Monte Carlo study, we vary the value of σ_E from 1% to 20% of the mean value of E in ten equally spaced linear steps. At each level of σ_E, we draw 1000 samples from the GP at the barycentres of each element, and from these compute the generalised eigenvalue decomposition, storing samples of the first (lowest) five eigenvalues and their corresponding eigenvectors.

To compare the Monte Carlo samples and the approximation we have developed, the first two moments of the samples are computed. However, for the eigenvectors, to arrive at sensible estimates of these moments, some post-processing of the samples has to be performed. Since the samples are eigenvectors, they may have arbitrary scaling or sign from the numerical eigendecomposition and still be valid eigenvectors of the system of equations defined by M and K. This scaling clearly will lead to biased estimates of the mean and covariance if computed from the samples directly. Therefore, we perform two normalisations to align the eigenvector samples as well as possible with each other. First, we remove any sign discrepancies in the samples. We do this by taking the dot product between the first sample for that eigenpair and all other samples, and then multiplying by the sign of the result. Secondly, we rescale all the resulting samples independently to have unit norm. Then we can compute the mean of the samples. The final stage where we must be careful is that when centring the eigenvector samples, we have to be mindful that they are now points on a hypersphere. Therefore, we project onto the tangent space of the mean eigenvector and compute the covariance from centred values in that tangent space.

We then use two different metrics for comparison of the eigenvalues and eigenvectors. For the mean of the eigenvectors, we compute the cosine similarity between the Monte Carlo mean and the estimate of the first moment from the Taylor series. In this case, a value of 1.0 indicates perfect alignment and 0.0 complete orthogonality; we choose this over the relative error used for the other quantities to respect the fact that the scaling of the eigenvectors could lead to high error despite good estimates. For the remaining estimates, we compare using the same relative error as Girolami et al. (2021); for each $\boldsymbol{q} \in \{\bar{\lambda}_i, C_{\lambda_i}, C_{\boldsymbol{\phi}_i}\}_{i=1}^5$, we compute the relative error ϵ,

$$\epsilon = \frac{||\boldsymbol{q} - \boldsymbol{q}^{(MC)}||_F}{||\boldsymbol{q}^{(MC)}||_F} \tag{25}$$

with $\boldsymbol{q}$ being the statFEM approximation and $\boldsymbol{q}^{(MC)}$ being the Monte Carlo estimate.

The results of this comparison are shown in Fig. 1. Errors for each of the first five eigenmodes are shown separately. We observe that the approximation of the first two moments that we have used is very good for the first five eigenvalues of the system. In the eigenvalues, we see some increase in error with an increase in the eigenvalue being considered, but this is not strictly the case; for example, $\bar{\lambda}_3$ shows lower relative error than $\bar{\lambda}_1$ across all levels of variance in the parameter E. Turning attention to the eigenvectors, in the mean estimate of the eigenvectors across the first five eigenmodes there is exceptional alignment according to the cosine similarity, which is above 0.999 for all levels of variance in E for each of these eigenmodes. Here we do see more clearly

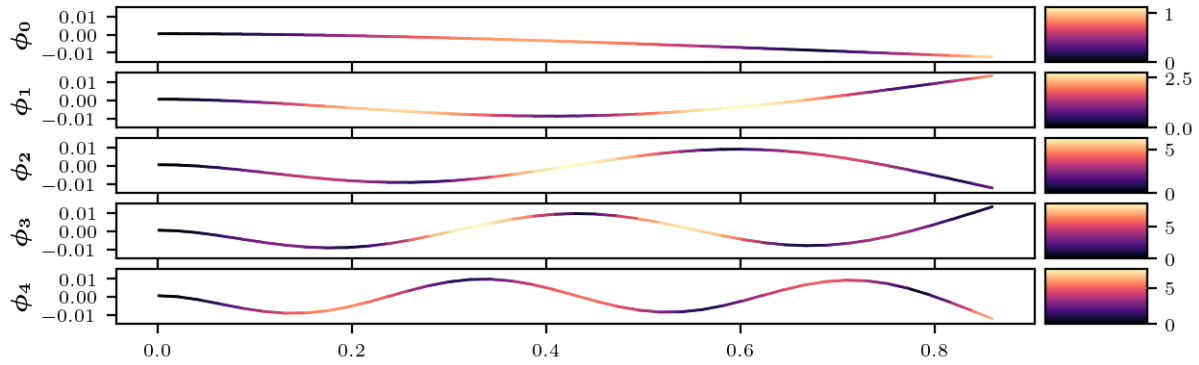

Figure 2: The first five eigenfunction solutions, deformation showing the expected shapes with colormap showing the marginal standard deviation ($\times 10^6$) of the mode shape at each node interpolated across the mesh.

that the estimates are becoming generally less effective with increasing eigenvalue, but the effect is small. The covariance error in the eigenvectors is a more interesting situation, where the error is broadly growing with increasing variance in E (as would be expected), but this is not happening monotonically or uniformly across these first five eigenmodes. We also see that relative error in the eigenvector covariance is higher than in the eigenvalues by approximately one order of magnitude; despite this, the relative errors we are observing here are comparable to the levels seen by Girolami et al. (2021) in the static statFEM case for the eigenvectors, while in the eigenvalues we see much smaller relative error.

We now present a case study on a more realistic engineering system (although it remains a simple one), again choosing the setup of a cantilevered beam. The beam is modelled as having a length of 0.86m and height of 0.001m, which define the rectangular domain of the beam, which is analysed using a two-dimensional solver. The domain is discretised into 120 elements, 40 along the beam's length and three across its height. The same element formulations as previously are used.

The thickness, density and Poisson's ratio for each element are considered known, and a random field is placed over the elastic modulus of the material such that it is varying across the domain. The elements are modelled as 0.025m thick with a density of $7850\mathrm{kg\,m^{-3}}$ and a Poisson's ratio of 0.33. These properties reflect standard values for a mild steel component.

The elastic (Young's) modulus E in GPa is chosen, as before, as the random parameter in the model, and a GP prior is placed over it identically to Eq. (23), keeping the covariance function as in Eq. (24). Setting $\bar{E} = 210\mathrm{GPa}$ to also match a typical set of properties for mild steel, we choose to demonstrate $\sigma_E = 21\mathrm{GPa}$ — a standard deviation of 10% of the mean value. Our choice aims to reflect variability that might arise in the manufacturing process for this type of metal component. The level of variability here is quite extreme compared to what may be seen in practice (2%–5%), but serves to demonstrate the utility of the presented method.

In Fig. 3, we show the approximate distributions over the first five eigenvalues of the beam computed by Eq. (15). As expected, we see strong positive correlation across

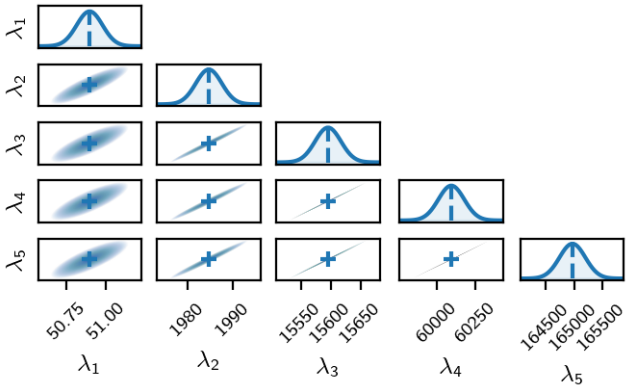

Figure 3: Covariances of the first five eigenfrequencies of the solution. Mean values are indicated with a dashed line.

the eigenvalue set. The corresponding eigenvectors of the solution (the "mode shapes") are also plotted in Fig. 2.

The eigenvectors are shown with the deformed mesh indicating the mean eigenvector solution and the colour map showing the variance over the eigenvector at each node, interpolated across the mesh. The distribution of the uncertainty across the eigenvectors may appear unintuitive. However, considering that the uncertainty is propagated via a Taylor series expansion, which relies on the gradients of the eigenvector, it is reasonable to see such a (spatial) distribution of uncertainty in the result. Of note, we see in modes three and four, the uncertainty is concentrated close to the nodal points (i.e. where the eigenvectors have values close to zero). The position of these nodal points is very sensitive to spatial variation in the system properties, which leads to high uncertainty around them.

Another interesting feature of the solution, which is apparent when considering the form of Eq. (20), is that there is coupling in the uncertainty between each of the eigenvectors. Equation (17) contains the expected eigenvectors from every eigenmode (and the associated expected eigenvalues); this ensures that there is information shared in the uncertainty between the eigenmodes. This sharing of information is likely responsible for the unintuitive increase in variance seen in mode one close to 0.35m along the length of the beam. Finally, we provide some additional results in Appendix E

showing the cross-covariances between the eigenvectors and eigenvalues.

5 Discussion

We have presented an approach that expands the applicability of statFEM methods to a wider community, those who wish to solve dynamic (vibration) problems. In this work, we have not directly addressed the case where an additional discrepancy function is added to the output of the dynamic statFEM model, but this follows trivially given the approximate Gaussian distributions shown for the eigenvectors and manifests as an additive covariance on the eigenvalues. The provision of this model for the eigendecomposition in statFEM analysis will allow the inclusion of uncertainty in many existing fields of engineering research. The analysis of the dynamic properties of a system is a vital step in the qualification of, e.g., automotive or aerospace systems; it also sees wide-reaching use in management and monitoring of civil infrastructure, and design of (for example) renewable energy systems such as wind turbines. In each of these applications, the quantification of uncertainty in these properties, as a result of spatially varying random parameters, is an important step in improving the robustness of the decisions made.

It is worth discussing at this point possible limitations or considerations that a practitioner should consider before applying the proposed formulation of statFEM to their problem. An important feature of the statFEM approach is to allow approximation of the distribution over the quantity of interest through the use of a Taylor series. This approach leads to a local Gaussian approximation of the true distribution over the displacement/dynamic properties. Owing to the nature of this approximation, the distributions will only be valid for small levels of uncertainty in $\boldsymbol{\theta}$, as in the original statFEM. For the dynamic vibration case presented in this work, the sensitivity of the output is higher than in the static statFEM case, especially with increasing eigenvalue.

Another limitation to consider in the specific form of statFEM presented here is that we are still adopting a Gaussian approximation to the distribution over the eigenvectors. Since the problem is a real-valued symmetric generalised eigenvalue problem, it is known that all of the eigenvalues should be real and positive and that the eigenvectors should be a set of real orthogonal vectors (by convention often orthonormal with respect to the mass matrix, i.e. $\Phi^{\mathrm{T}} M \Phi = \mathbb{I}$). Under the Gaussian approximation, neither of these properties is preserved by construction, some further discussion is presented in Appendix F. Although for the case shown in this study, the probability of negative eigenvalues is very low, it should be noted that there is a non-zero probability of this solution. Both of these issues may be exacerbated if a discrepancy model is additionally applied. Where to place the discrepancy model in this analysis should be carefully considered by the practitioner. Mathematically, there is no reason not to include this over the eigenvectors themselves as an additional covariance from an additive GP; however, caution should be exercised that results stay true to the engineering inductive biases. Alternatively, the discrepancy could be delayed and included at the time-series level when performing simulation, which would avoid this issue but would not give information about the "corrected" eigenvectors, which are likely of interest.

It is also clear that the desire for orthogonality of the eigenvectors places another limit on the level of uncertainty in $\boldsymbol{\theta}$ for which the approximate solution is valid. For the eigenvectors, the Gaussian distributions over them — even given the influence of the other eigenpairs on the covariance — will not guarantee that samples remain orthogonal between $\boldsymbol{\phi}_i$ and $\boldsymbol{\phi}_j$. In practice, since the levels of uncertainty have to remain small for the Taylor series approximation, this may not be a major barrier in practical application. In the results, it has been seen that the estimated mean and covariances remain close to the Monte Carlo results, where the vectors are orthogonal by construction. For example, in the inverse problem where eigenfunctions of these systems are recovered by "Modal Analysis" (see Ewins (2009)), the eigenfunctions/eigenvectors are only observed at a small number of discrete locations within the domain and (to our knowledge) orthogonality conditions on the eigenfunction across the whole domain are not enforced. Similarly, if the results of this statFEM approximation were used to assist in sensor placement optimisation, knowledge of the covariance of the eigenvectors may well be sufficient to inform better strategies than solely relying on the solution using mean parameter values.

We can also consider how the results demonstrated here might be used in the inverse problem setting. Unlike the usual statFEM construction, although a discrepancy function can be easily added, it is not so clear that there would not be additional complications in the inference. The principal problem will be that it is not usually possible to observe directly the eigenfrequencies or eigenvectors of a physical system, so the observation process will be somewhat more complicated. Therefore, in practice, the formulation we present in this work would have to form part of a wider hierarchical Bayesian model that also included the generative model from the properties (eigenpairs) to the observation space, usually time-series of accelerations at a small number of fixed locations in the domain.

Finally, the results of the presented statFEM approach would allow for uncertainty in system properties to be propagated forward onto time-series simulations of the dynamics (under linear dynamic assumptions) through the construction of linear superposition models. The response of the system may be simulated as the response of a set of harmonic oscillators with frequencies given by the eigenfrequencies (square roots of the eigenvalues); then, these "modal responses" may be combined through the eigenvectors to describe motion across the whole domain. Care must be taken in the simulation of the harmonic oscillator with a random resonant frequency, but this can be achieved in an approximate way by assuming Gaussian transition densities in a time-stepping model.

6 Conclusion

In this work, a new statFEM formulation for solving "modal vibration" problems has been presented, where the practitioner is interested in the eigendecomposition of the discretised mass and stiffness of the FE model. These results are especially of interest to applications in the structural dynamics and control communities, although they have applications in many engineering settings. We have shown that the fundamental tools of statFEM, specifically in relation to the Taylor series approximation of the uncertainty propagated through the FE solution, can be readily used in the dynamic vibration case. We have provided expressions that allow for a Gaussian approximation of the distribution of the eigenvalues and associated eigenvectors given parameters that are varying *a priori* as a random field, modelled using a Gaussian process. We have also noted several limitations of the approach adopted here, which motivate further work into an improved approximation of the distributions and the inclusion of this model form in wider Bayesian frameworks.

Acknowledgements

TJR and BJOC acknowledge support for this work as part of EPSRC Programme Grant ROSEHIPS (grant no. EP/W005816/1), and TJR additionally through the ATI project OLLGA (grant no. 10040817). MDC is grateful for the support of the University of Sheffield through the Centre for Machine Intelligence.

References

S. Adhikari. Rates of change of eigenvalues and eigenvectors in damped dynamic system. *AIAA Journal*, 37:1452–1458, 1999. doi: 10.2514/2.622.

S. Adhikari and M. Friswell. Random matrix eigenvalue problems in structural dynamics. *International Journal for Numerical Methods in Engineering*, 69 (3):562–591, 2007.

Ö. D. Akyildiz, C. Duffin, S. Sabanis, and M. Girolami. Statistical finite elements via langevin dynamics. *SIAM/ASA Journal on Uncertainty Quantification*, 10(4):1560–1585, 2022.

R. Barros, I. Rocha, M. N. Macho, and O. M. Napoles. Forward uncertaint propagation for finite element models with non-Gaussian parameters. In *UNCECOMP 2025 6th ECCOMAS Thematic Conference on Uncertainty Quantification in Computational Sciences and Engineering*, 2025.

K.-J. Bathe. *Finite element procedures*. Prentice Hall, 2006.

J. Bradbury, R. Frostig, P. Hawkins, M. J. Johnson, Y. Katariya, C. Leary, D. Maclaurin, G. Necula, A. Paszke, J. VanderPlas, S. Wanderman-Milne, and Q. Zhang. JAX: composable transformations of Python+NumPy programs, 2018. URL http://github.com/jax-ml/jax.

A. Cicirello and R. S. Langley. The vibro-acoustic analysis of built-up systems using a hybrid method with parametric and non-parametric uncertainties. *Journal of Sound and Vibration*, 332(9):2165–2178, 2013.

C. Duffin, E. Cripps, T. Stemler, and M. Girolami. Low-rank statistical finite elements for scalable model-data synthesis. *Journal of Computational Physics*, 463:111261, 2022.

C. Duffin, A. Glyn-Davies, A. Vadeboncoeur, and M. Girolami. The statistical finite element method: A theoretical foundation for digital twins. *Quality Engineering*, 38(1):112–121, 2026.

D. J. Ewins. *Modal testing: theory, practice and application*. John Wiley & Sons, 2009.

E. Febrianto, L. Butler, M. Girolami, and F. Cirak. Digital twinning of self-sensing structures using the statistical finite element method. *Data-Centric Engineering*, 3:e31, 2022.

M. Girolami, E. Febrianto, G. Yin, and F. Cirak. The statistical finite element method (statfem) for coherent synthesis of observation data and model predictions. *Computer Methods in Applied Mechanics and Engineering*, 375:113533, 2021.

P. Hennig, M. A. Osborne, and M. Girolami. Probabilistic numerics and uncertainty in computations. *Proceedings of the Royal Society A: Mathematical, Physical and Engineering Sciences*, 471(2179), 2015.

M. C. Kennedy and A. O'Hagan. Bayesian calibration of computer models. *Journal of the Royal Statistical Society: Series B (Statistical Methodology)*, 63(3): 425–464, 2001.

W. K. Liu, T. Belytschko, and A. Mani. Random field finite elements. *International journal for numerical methods in engineering*, 23(10):1831–1845, 1986.

R. B. Nelson. Simplified calculation of eigenvector derivatives. *AIAA Journal*, 14:1201–1205, 1976. doi: 10.2514/3.7211.

Y. Papandreou, J. Cockayne, M. Girolami, and A. Duncan. Theoretical guarantees for the statistical finite element method. *SIAM/ASA Journal on Uncertainty Quantification*, 11(4):1278–1307, 2023.

S. S. Rao and F. F. Yap. *Mechanical vibrations*, volume 4. Addison-Wesley New York, 1995.

C. Soize. Random matrix theory for modeling uncertainties in computational mechanics. *Computer methods in applied mechanics and engineering*, 194(12-16): 1333–1366, 2005.

F. Sun, E. Febrianto, H. Fernando, L. J. Butler, F. Cirak, and N. A. Hoult. Data-informed statistical finite element analysis of rail buckling. *Computers & Structures*, 289:107163, 2023.

A Modal Analysis in Structural Dynamics

This section presents a brief introduction to the concept of modal analysis in structural dynamics for readers who may be unfamiliar with the field. For a comprehensive treatment, we direct the reader to Ewins (2009) as a key reference.

The foundational principle underpinning this approach is that the dynamic response of a linear system can be expressed as a superposition of its responses in each of its individual (eigen-)modes. Consider a discrete lumped-mass system whose equation of motion is given by

$$M\ddot{\boldsymbol{x}}(t) + K\boldsymbol{x}(t) = \boldsymbol{f}(t), \tag{26}$$

where $M, K \in \mathbb{R}^{N\times N}$ are symmetric positive-definite mass and stiffness matrices, $\boldsymbol{x}(t) \in \mathbb{R}^N$ is the vector of displacements, and $\boldsymbol{f}(t) \in \mathbb{R}^N$ represents external forcing. We can introduce a coordinate transformation $\boldsymbol{x}(t) = \Phi\boldsymbol{q}(t)$ and pre-multiply Eq. (26) by Φ^{T}:

$$\Phi^{\mathrm{T}}M\Phi\ddot{\boldsymbol{q}}(t) + \Phi^{\mathrm{T}}K\Phi\boldsymbol{q}(t) = \Phi^{\mathrm{T}}\boldsymbol{f}(t). \tag{27}$$

When the columns of $\Phi = [\boldsymbol{\phi}_1, \ldots, \boldsymbol{\phi}_N]$ are the eigenvectors of the generalised eigenvalue problem

$$K\boldsymbol{\phi}_i = \lambda_i M\boldsymbol{\phi}_i, \tag{28}$$

the matrices M and K are simultaneously diagonalised due to orthogonality ($\boldsymbol{\phi}_i^{\mathrm{T}}M\boldsymbol{\phi}_j = \delta_{ij}$ and $\boldsymbol{\phi}_i^{\mathrm{T}}K\boldsymbol{\phi}_j = \lambda_i\delta_{ij}$). This completely decouples the system of equations. Here, we are assuming the "mass-normalised" scaling of the eigenvectors such that $\Phi^{\mathrm{T}}M\Phi = \mathbb{I}$.

This transformation provides a very intuitive physical interpretation of the system response. At any degree of freedom, the total motion is a linear combination of the responses of N independent single-degree-of-freedom harmonic oscillators, combined according to the spatial values of the eigenvectors.

Two critical properties arise from this process. First, each independent oscillator possesses a natural resonant frequency $\omega_i = \sqrt{\lambda_i}$. Consequently, a system with N degrees of freedom possesses N natural frequencies (which are generally unique in practice, though physical symmetries can introduce repeated eigenvalues). Second, the eigenvectors $\boldsymbol{\phi}_i$—frequently referred to as *mode shapes*—describe the characteristic spatial patterns of vibration when the system resonates at the corresponding eigenfrequency.

This analysis extends naturally to continuous problems governed by PDEs, the classic example being the wave equation describing the transverse motion of a vibrating string under small deflections. Separation of variables yields an infinite set of discrete eigenvalues and continuous spatial eigenfunctions $\phi_i(x)$ in place of discrete eigenvectors. Here, a major benefit of modal analysis becomes clear: it cleanly separates the spatial and temporal dynamics. The temporal behaviour is governed by independent one-dimensional harmonic oscillators $q_i(t)$, while the spatial distribution is captured entirely by the eigenfunctions $\phi_i(x)$.

Although a continuous string possesses infinitely many eigenfrequencies, truncating the expansion to a finite set of Q modes provides a principled, physics-informed method to control computational complexity while preserving spatial fidelity. In engineering applications, the spectral bandwidth of expected excitation loads can directly inform how many modes Q must be retained. Crucially, when solving large PDEs approximately using the FEM, one needs to solve the large generalised eigenvalue problem only once; subsequent time-stepping or probabilistic simulations can be performed at low cost in the reduced Q-dimensional modal space before mapping the solution back to the full spatial field.

B Series Approximation in statFEM

To arrive at expressions for the approximate first and second moments of the eigenvalues and eigenvectors, it is clearest to first consider the Taylor series approximation to a general quantity of interest $\boldsymbol{q}$, which is computed via a FEM procedure. This approach follows the results that are also found in Liu et al. (1986).

We will also consider the case where the FE solution is governed by some parameter(s) $\boldsymbol{\theta}$ that vary over the domain of the model with a prescribed (prior) distribution

$$\boldsymbol{\theta} \sim \mathcal{GP}\left(\bar{\boldsymbol{\theta}}(\boldsymbol{x}), c_{\boldsymbol{\theta}}(\boldsymbol{x}, \boldsymbol{x}')\right) \tag{29}$$

for two points in the domain $\boldsymbol{x}$ and $\boldsymbol{x}'$.

Note that $\boldsymbol{\theta}$ may be vector-valued if a suitable multiple-output GP can be defined. The goal of this analysis will be to arrive at an approximation to the quantity of interest, which is some nonlinear transform (through the FE model) of the random field $\boldsymbol{\theta}$, $\boldsymbol{q} = \varphi(\boldsymbol{\theta})$.

The approximation that we will target is

$$p(\boldsymbol{q}) = \int p(\boldsymbol{q}|\boldsymbol{\theta})p(\boldsymbol{\theta})\mathrm{d}\boldsymbol{\theta} \approx \mathcal{N}(\bar{\boldsymbol{q}}, C_{\boldsymbol{q}}) \tag{30}$$

From the construction of the FEM solution as a summation over elements and choosing to truncate the Taylor series at the first order, we can write,

$$\boldsymbol{q} \approx \varphi(\bar{\boldsymbol{\theta}}) + \sum_{e=1}^{n_e} \left.\frac{\partial\varphi(\boldsymbol{\theta})}{\partial\boldsymbol{\theta}_e}\right|_{\bar{\boldsymbol{\theta}}} (\boldsymbol{\theta}_e - \bar{\boldsymbol{\theta}}_e), \tag{31}$$

for n_e elements in the mesh and (as in Girolami et al. (2021)) considering the value of the random field at the barycentre of the elements, which we will define as $\boldsymbol{x}_e^{(c)}$ for the e^{th} element, with $\boldsymbol{\theta}_e$ being the random variable $\boldsymbol{\theta}\left(\boldsymbol{x}_e^{(c)}\right)$, and $\bar{\boldsymbol{\theta}}_e$ being its mean.

To approximate the first moment of $\boldsymbol{q}$ ($\bar{\boldsymbol{q}}$), we take expectations over this Taylor series expansion,

$$\bar{\boldsymbol{q}} = \mathbb{E}\left[\varphi(\bar{\boldsymbol{\theta}}) + \sum_{e=1}^{n_e} \left.\frac{\partial\varphi(\boldsymbol{\theta})}{\partial\boldsymbol{\theta}_e}\right|_{\bar{\boldsymbol{\theta}}} (\boldsymbol{\theta}_e - \bar{\boldsymbol{\theta}}_e)\right] = \varphi(\bar{\boldsymbol{\theta}}). \tag{32}$$

Then for the covariance of $\boldsymbol{q}$, by definition, we know this should equal

$$\mathbb{V}[\boldsymbol{q}] = \mathbb{E}\left[(\boldsymbol{q} - \bar{\boldsymbol{q}}) \otimes (\boldsymbol{q} - \bar{\boldsymbol{q}})\right]. \tag{33}$$

Substituting in the expressions for the Taylor series expansion and the previous result for $\bar{\boldsymbol{q}}$,

$$C_{\boldsymbol{q}} = \mathbb{E}\left[\left(\sum_{e=1}^{n_e} \frac{\partial\varphi(\boldsymbol{\theta})}{\partial\boldsymbol{\theta}_e}\bigg|_{\bar{\boldsymbol{\theta}}} (\boldsymbol{\theta}_e - \bar{\boldsymbol{\theta}}_e)\right) \otimes \left(\sum_{d=1}^{n_e} \frac{\partial\varphi(\boldsymbol{\theta})}{\partial\boldsymbol{\theta}_d}\bigg|_{\bar{\boldsymbol{\theta}}} (\boldsymbol{\theta}_d - \bar{\boldsymbol{\theta}}_d)\right)\right]. \tag{34}$$

$$C_{\boldsymbol{q}} = \sum_{e=1}^{n_e}\sum_{d=1}^{n_e} \frac{\partial\varphi(\boldsymbol{\theta})}{\partial\boldsymbol{\theta}_e}\bigg|_{\bar{\boldsymbol{\theta}}} C_{ed}^{\boldsymbol{\theta}} \left(\frac{\partial\varphi(\boldsymbol{\theta})}{\partial\boldsymbol{\theta}_d}\bigg|_{\bar{\boldsymbol{\theta}}}\right)^{\mathrm{T}} \tag{35}$$

with $C_{ed}^{\boldsymbol{\theta}} = c_{\boldsymbol{\theta}}(\boldsymbol{x}_e^{(c)}, \boldsymbol{x}_d^{(c)})$, again by definition of the covariance of $\boldsymbol{\theta}$.

From the final expressions in Eqs. (32) and (35), it can be seen that the approximate mean is simply the FE model evaluated at the mean of the random field, and that the covariance will be dependent on only the covariance of the random parameter field and the Jacobians of the nonlinear transform with respect to the parameters evaluated at the mean.

In practice, this means that the challenge in extending statFEM to alternative outputs from the FE model, e.g. the eigendecomposition, is to be able to express the Jacobian

$$\frac{\partial\varphi(\boldsymbol{\theta})}{\partial\boldsymbol{\theta}_e}\bigg|_{\bar{\boldsymbol{\theta}}}. \tag{36}$$

C Derivatives of the Eigendecomposition

In Section 3, forming the Taylor series approximations for the covariance matrices of the eigenvectors—given in Eqs. (15) and (20)—requires evaluating the first-order partial derivatives of the generalised eigenvalue problem with respect to the spatial parameter field components θ_e.

We start from the deterministic generalised eigenvalue problem evaluated at the mean parameter field $\bar{\boldsymbol{\theta}}$:

$$\bar{K}\bar{\boldsymbol{\phi}}_i = \bar{\lambda}_i \bar{M}\bar{\boldsymbol{\phi}}_i, \quad i = 1, \ldots, Q, \tag{37}$$

where $\bar{K} \triangleq K(\bar{\boldsymbol{\theta}})$ and $\bar{M} \triangleq M(\bar{\boldsymbol{\theta}})$ are real symmetric matrices, and the eigenvectors satisfy the mass orthonormality condition $\bar{\boldsymbol{\phi}}_i^{\mathrm{T}}\bar{M}\bar{\boldsymbol{\phi}}_j = \delta_{ij}$ (or compactly, $\bar{\Phi}^{\mathrm{T}}\bar{M}\bar{\Phi} = \mathbb{I}$).

C.1 Eigenvalue Derivatives

Differentiating Eq. (37) with respect to parameter θ_e evaluated at $\bar{\boldsymbol{\theta}}$ yields:

$$\frac{\partial\bar{K}}{\partial\theta_e}\bar{\boldsymbol{\phi}}_i + \bar{K}\frac{\partial\bar{\boldsymbol{\phi}}_i}{\partial\theta_e} = \frac{\partial\bar{\lambda}_i}{\partial\theta_e}\bar{M}\bar{\boldsymbol{\phi}}_i + \bar{\lambda}_i\frac{\partial\bar{M}}{\partial\theta_e}\bar{\boldsymbol{\phi}}_i + \bar{\lambda}_i\bar{M}\frac{\partial\bar{\boldsymbol{\phi}}_i}{\partial\theta_e}. \tag{38}$$

Pre-multiplying Eq. (38) by $\bar{\boldsymbol{\phi}}_i^{\mathrm{T}}$ gives:

$$\bar{\boldsymbol{\phi}}_i^{\mathrm{T}}\frac{\partial\bar{K}}{\partial\theta_e}\bar{\boldsymbol{\phi}}_i + \bar{\boldsymbol{\phi}}_i^{\mathrm{T}}\bar{K}\frac{\partial\bar{\boldsymbol{\phi}}_i}{\partial\theta_e} = \frac{\partial\bar{\lambda}_i}{\partial\theta_e}\bar{\boldsymbol{\phi}}_i^{\mathrm{T}}\bar{M}\bar{\boldsymbol{\phi}}_i + \bar{\lambda}_i\bar{\boldsymbol{\phi}}_i^{\mathrm{T}}\frac{\partial\bar{M}}{\partial\theta_e}\bar{\boldsymbol{\phi}}_i + \bar{\lambda}_i\bar{\boldsymbol{\phi}}_i^{\mathrm{T}}\bar{M}\frac{\partial\bar{\boldsymbol{\phi}}_i}{\partial\theta_e}. \tag{39}$$

Due to the symmetry of $\bar{K}$ and $\bar{M}$, we have the identity $\bar{\boldsymbol{\phi}}_i^{\mathrm{T}}\bar{K} = \bar{\lambda}_i\bar{\boldsymbol{\phi}}_i^{\mathrm{T}}\bar{M}$, which causes the terms involving the eigenvector derivative $\frac{\partial\bar{\boldsymbol{\phi}}_i}{\partial\theta_e}$ on both sides of the equation to cancel identically. Applying the mass-normalisation condition $\bar{\boldsymbol{\phi}}_i^{\mathrm{T}}\bar{M}\bar{\boldsymbol{\phi}}_i = 1$, we recover the first-order eigenvalue derivative:

$$\frac{\partial\bar{\lambda}_i}{\partial\theta_e} = \bar{\boldsymbol{\phi}}_i^{\mathrm{T}}\left(\frac{\partial\bar{K}}{\partial\theta_e} - \bar{\lambda}_i\frac{\partial\bar{M}}{\partial\theta_e}\right)\bar{\boldsymbol{\phi}}_i, \tag{40}$$

which provides the inner product required for the eigenvalue covariance sum in Eq. (15).

C.2 Eigenvector Derivatives

To determine the eigenvector derivative $\frac{\partial\bar{\boldsymbol{\phi}}_i}{\partial\theta_e}$, we follow classical modal sensitivity and algebraic formulations (Nelson, 1976; Adhikari, 1999). Assuming distinct eigenvalues, the derivative of the i^{th} eigenvector can be expressed as a linear combination of the complete basis:

$$\frac{\partial\bar{\boldsymbol{\phi}}_i}{\partial\theta_e} = \sum_{k=1}^{N} c_{ik}^{(e)}\bar{\boldsymbol{\phi}}_k = \bar{\Phi}\boldsymbol{c}_i^{(e)}. \tag{41}$$

Substituting Eq. (41) into Eq. (38) and pre-multiplying by $\bar{\boldsymbol{\phi}}_j^{\mathrm{T}}$ (where $j \neq i$) yields:

$$\bar{\boldsymbol{\phi}}_j^{\mathrm{T}}\left(\bar{K} - \bar{\lambda}_i\bar{M}\right)\bar{\Phi}\boldsymbol{c}_i^{(e)} = -\bar{\boldsymbol{\phi}}_j^{\mathrm{T}}\left(\frac{\partial\bar{K}}{\partial\theta_e} - \bar{\lambda}_i\frac{\partial\bar{M}}{\partial\theta_e}\right)\bar{\boldsymbol{\phi}}_i. \tag{42}$$

Invoking mass orthogonality $\bar{\boldsymbol{\phi}}_i^{\mathrm{T}}\bar{M}\bar{\boldsymbol{\phi}}_j = \delta_{ij}$ and $\bar{\boldsymbol{\phi}}_i^{\mathrm{T}}\bar{K}\bar{\boldsymbol{\phi}}_j = \bar{\lambda}_i\delta_{ij}$, the left-hand side reduces to $(\bar{\lambda}_j - \bar{\lambda}_i)c_{ij}^{(e)}$, giving the off-diagonal coefficients:

$$c_{ij}^{(e)} = -\frac{1}{\bar{\lambda}_j - \bar{\lambda}_i}\bar{\boldsymbol{\phi}}_j^{\mathrm{T}}\left(\frac{\partial\bar{K}}{\partial\theta_e} - \bar{\lambda}_i\frac{\partial\bar{M}}{\partial\theta_e}\right)\bar{\boldsymbol{\phi}}_i, \quad j \neq i. \tag{43}$$

To find the diagonal coefficient $c_{ii}^{(e)}$, we differentiate the mass-normalisation identity $\bar{\boldsymbol{\phi}}_i^{\mathrm{T}}\bar{M}\bar{\boldsymbol{\phi}}_i = 1$ with respect to θ_e:

$$2\bar{\boldsymbol{\phi}}_i^{\mathrm{T}}\bar{M}\frac{\partial\bar{\boldsymbol{\phi}}_i}{\partial\theta_e} + \bar{\boldsymbol{\phi}}_i^{\mathrm{T}}\frac{\partial\bar{M}}{\partial\theta_e}\bar{\boldsymbol{\phi}}_i = 0. \tag{44}$$

Substituting Eq. (41) and applying $\bar{\boldsymbol{\phi}}_i^{\mathrm{T}}\bar{M}\bar{\boldsymbol{\phi}}_k = \delta_{ik}$ yields:

$$c_{ii}^{(e)} = -\frac{1}{2}\bar{\boldsymbol{\phi}}_i^{\mathrm{T}}\frac{\partial\bar{M}}{\partial\theta_e}\bar{\boldsymbol{\phi}}_i. \tag{45}$$

We can now re-assemble the full eigenvector derivative vector into a compact matrix expression. Defining the diagonal matrix of mean eigenvalues $\bar{\Lambda} = \mathrm{diag}(\bar{\lambda}_1, \ldots, \bar{\lambda}_Q)$, the Moore-Penrose pseudo-inverse $(\bar{\Lambda} - \bar{\lambda}_i\mathbb{I})^{\dagger}$ has diagonal entries $(\bar{\lambda}_j - \bar{\lambda}_i)^{-1}$ for $j \neq i$ and 0 for $j = i$. Thus, defining the projection matrix

$$F_i = -\bar{\Phi}\left(\bar{\Lambda} - \bar{\lambda}_i\mathbb{I}\right)^{\dagger}\bar{\Phi}^{\mathrm{T}}, \tag{46}$$

as in Eq. (17), applies the exact weighting required for all $j \neq i$ components while mapping the $j = i$ component to zero. Combining this with the diagonal contribution $c_{ii}^{(e)}$, we define the complete sensitivity forcing vector D_{ei} as:

$$D_{ei} = \left(\frac{\partial\bar{K}}{\partial\theta_e} - \bar{\lambda}_i\frac{\partial\bar{M}}{\partial\theta_e}\right)\bar{\boldsymbol{\phi}}_i - \frac{1}{2}\left(\bar{\boldsymbol{\phi}}_i^{\mathrm{T}}\frac{\partial\bar{M}}{\partial\theta_e}\bar{\boldsymbol{\phi}}_i\right)\bar{M}\bar{\boldsymbol{\phi}}_i, \tag{47}$$

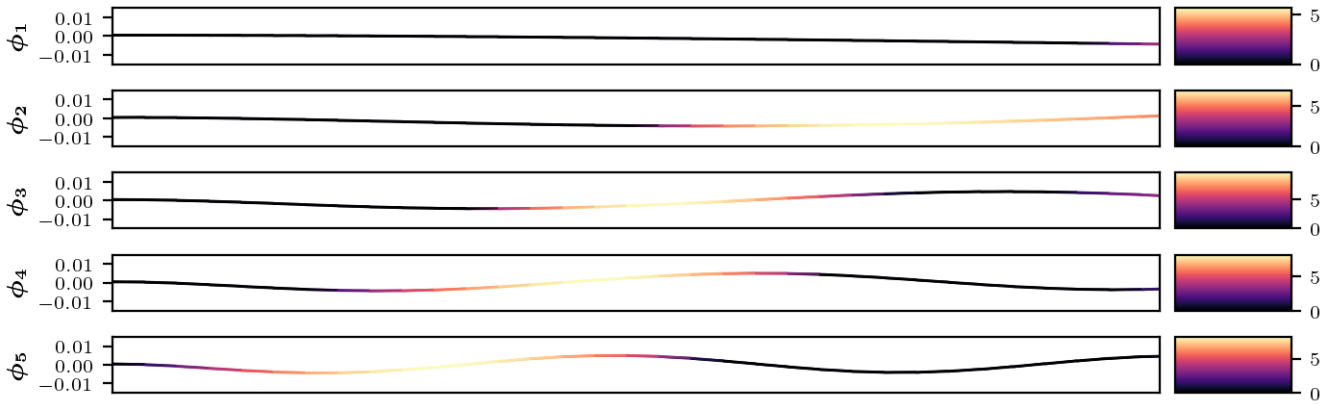

Figure 4: The first five eigenfunction solutions, deformation showing the expected shapes with colormap showing the standard deviation ($\times 10^5$) marginally at each node of the cross covariance between that eigenvector and the fifth eigenvalue.

such that the first-order eigenvector derivative evaluated at the mean parameter field is compactly expressed as:

$$\frac{\partial \bar{\boldsymbol{\phi}}_i}{\partial \theta_e} = F_i D_{ei}, \tag{48}$$

which directly underpins the eigenvector covariance approximation in Eq. (20).

D Quadrilateral Elements

The elements used throughout this work are chosen to be 8-noded quadrilateral elements. These elements are quadrilateral with four nodal points defining the corners of the element and with additional nodes placed at the midpoint of each side. This element allows the use of second-order shape functions, which show improved efficiency in the FEM approximation.

In natural coordinates (ξ, η), the shape functions of the element used are as follows:

$$N_1(\xi,\eta) = \frac{1}{4}(1-\xi)(1-\eta)(-\xi-\eta-1), \tag{49a}$$
$$N_2(\xi,\eta) = \frac{1}{2}(1-\xi^2)(1-\eta), \tag{49b}$$
$$N_3(\xi,\eta) = \frac{1}{4}(1+\xi)(1-\eta)(\xi-\eta-1), \tag{49c}$$
$$N_4(\xi,\eta) = \frac{1}{2}(1+\xi)(1-\eta^2), \tag{49d}$$
$$N_5(\xi,\eta) = \frac{1}{4}(1+\xi)(1+\eta)(\xi+\eta-1), \tag{49e}$$
$$N_6(\xi,\eta) = \frac{1}{2}(1-\xi^2)(1+\eta), \tag{49f}$$
$$N_7(\xi,\eta) = \frac{1}{4}(1-\xi)(1+\eta)(-\xi+\eta-1), \tag{49g}$$
$$N_8(\xi,\eta) = \frac{1}{2}(1-\xi)(1-\eta^2). \tag{49h}$$

For the computation of the element stiffness matrices, we use the usual plane-stress constitutive matrix

$$D = \frac{E}{1-\nu^2}\begin{bmatrix} 1 & \nu & 0 \\ \nu & 1 & 0 \\ 0 & 0 & \frac{1}{2}(1-\nu) \end{bmatrix} \tag{50}$$

with $\nu = 0.33$ for all experiments in this work. The element stiffness matrix is computed as,

$$k_e = \int_{-1}^{1}\int_{-1}^{1} B(\xi,\eta)^{\mathrm{T}} D B(\xi,\eta)\, t\, |J|\, \mathrm{d}\xi\, \mathrm{d}\eta, \tag{51}$$

which is evaluated via a 9-point Gauss quadrature for elements of a uniform thickness t. $|J|$ is the determinant of the Jacobian, which accounts for the scale change between the global and natural coordinates, and B is the strain-displacement matrix.

$$B(\xi,\eta) = \begin{bmatrix} \frac{\partial N_1}{\partial x} & 0 & \dots & \frac{\partial N_8}{\partial x} & 0 \\ 0 & \frac{\partial N_1}{\partial y} & \dots & 0 & \frac{\partial N_8}{\partial y} \\ \frac{\partial N_1}{\partial y} & \frac{\partial N_1}{\partial x} & \dots & \frac{\partial N_8}{\partial y} & \frac{\partial N_8}{\partial x} \end{bmatrix} \tag{52}$$

which is computable from the partial derivatives with respect to the natural coordinates ξ and η multiplied by the inverse of the Jacobian,

$$J = \begin{bmatrix} \frac{\partial x}{\partial \xi} & \frac{\partial y}{\partial \xi} \\ \frac{\partial x}{\partial \eta} & \frac{\partial y}{\partial \eta} \end{bmatrix}, \tag{53}$$

E Vector-Value Cross Covariance

In the main body, we have focussed on the (approximate) marginal distributions over the eigenvalues $p(\boldsymbol{\lambda})$ and $p(\Phi)$. In the results, the joint distribution over all the eigenvalues has been discussed, and the figures have shown the marginal variance of the approximate eigenvector distributions, i.e.

$$\mathrm{Cov}(\boldsymbol{\phi}_i, \boldsymbol{\phi}_i) = \sum_{e=1}^{n_e}\sum_{d=1}^{n_e} F_i D_{ei} \tilde{C}_{ii}^{(ed)} D_{di}^{\mathrm{T}} F_i^{\mathrm{T}}. \tag{54}$$

However, following Appendix B, we can also construct approximations to the cross-covariances between the eigenvalues and eigenvectors.

$$\mathrm{Cov}(\boldsymbol{\phi}_i, \lambda_j) = \sum_{e=1}^{n_e}\sum_{d=1}^{n_e} F_i D_{ei} \tilde{C}_{ij}^{(ed)} \left[\bar{\boldsymbol{\phi}}_j^{\mathrm{T}} \left(\frac{\partial \bar{K}}{\partial \theta_d} - \bar{\lambda}_j \frac{\partial \bar{M}}{\partial \theta_d}\right) \bar{\boldsymbol{\phi}}_j\right]. \tag{55}$$

In Fig. 4, we show one example of this computation for the same case study as the main body. The variances at each node are shown for the cross-covariance

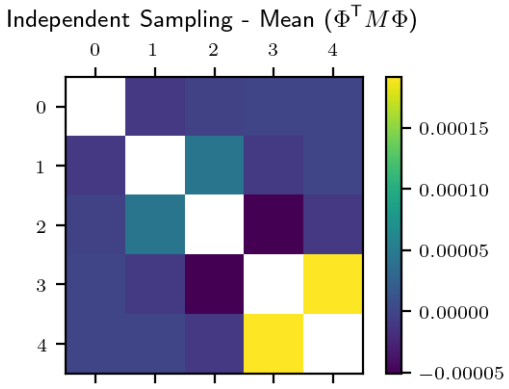

Figure 5: Mean values of the scaled inner product pairwise between samples of the eigenvectors when each eigenvector is sampled independently.

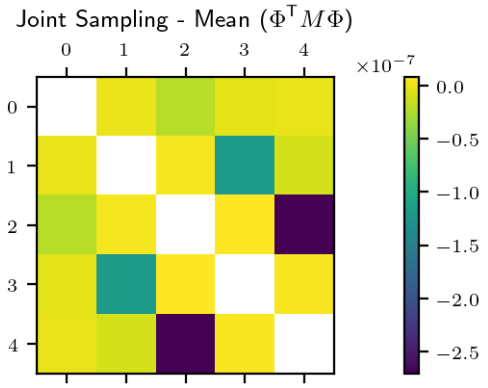

Figure 6: Mean values of the scaled inner product pairwise between samples of the eigenvectors when each eigenvector is sampled jointly.

of the first five eigenvectors with the fifth eigenvalue, i.e. $\mathrm{Cov}(\boldsymbol{\phi}_i, \lambda_5)$ for $i = 1, \ldots, 5$.

Despite λ_5 being a scalar, it is possible to see that the variance in the mode shapes is spatially correlated. This is a result of the inherent coupling between the eigenvalues and eigenvectors, which share the same stiffness and mass matrices. It is clear from the formulation in Eq. (55) that we will observe an interdependence between the eigenvalue and the eigenvectors in space, since the associated mean eigenvector $\bar{\boldsymbol{\phi}}_j$ appears in the gradient expressions on the right-hand side of the covariance.

F Eigenvector Orthogonality

It has been discussed that we are unable in this work to enforce, by construction, that the distributions of the eigenvectors will return samples that remain orthogonal with respect to the mass matrix (or equivalently the stiffness matrix). Here, we perform a short study to investigate the level to which we observe this loss of orthogonality in samples from the approximate Gaussian distributions that we derive in this work.

To check the extent to which this condition is being violated, we perform a small Monte Carlo study where we draw samples from the approximated distribution over the eigenvectors and calculate the quantity $\Phi^T M \Phi$, which should be equal to the identity matrix given our belief about orthogonality and the mass scaling applied to the eigenvectors.

In Fig. 5, we show this for the case where we sample from each of the eigenvectors independently, i.e. we compute $\mathrm{Cov}(\boldsymbol{\phi}_i, \boldsymbol{\phi}_i)$ and assume $\mathrm{Cov}(\boldsymbol{\phi}_i, \boldsymbol{\phi}_j) = 0$. The diagonal is removed, since this was unity within machine precision and it obscured the off-diagonal information, which encodes how far from orthogonal two eigenvectors are. We sample fifty independent realisations of each eigenvector from the approximate Gaussian distribution and plot the average over the resulting values for $\Phi^T M \Phi$. The samples remain very close to orthogonal in this case, considering no cross-correlation between eigenpairs is accounted for and the samples are drawn from Gaussian distributions. This result would seem to confirm that the approximation provided by statFEM in this instance is reasonable.

However, it is possible to improve quite significantly on this result by sampling jointly across all the eigenvectors if one computes all the pairwise $\mathrm{Cov}(\boldsymbol{\phi}_i, \boldsymbol{\phi}_j)$. The result of considering the full joint distribution $p(\Phi)$ is shown in Fig. 6. Note that the scaled inner products reduce to the order of 10^{-7}, which for an engineering context is very close to orthogonal and would not cause large concerns from the physical interpretation of these quantities. It should be noted that there is clearly an increased computational cost associated with calculating all of the cross-covariances $\mathrm{Cov}(\boldsymbol{\phi}_i, \boldsymbol{\phi}_j)$ for $i \neq j$, which is avoided in the independent case, and also the cost of sampling increases, since now we must sample from a covariance matrix that is $QN \times QN$ rather than sampling from Q independent $N \times N$ covariances. Therefore, the use-case must dictate the most appropriate choices for the modeller.